I&EC research
Industrial & Engineering Chemistry Research

ARTICLE

pubs.acs.org/IECR

Reactor Designs for Ethylene Production via Ethane Oxidative Dehydrogenation: Comparison of Performance

María L. Rodríguez,*[,†,‡] Daniel E. Ardissone,[‡] Eduardo López,[†,§] Marisa N. Pedernera,[†] and Daniel O. Borio[†]

[†]PLAPIQUI (UNS-CONICET), Camino La Carrindanga, km. 7, 8000 Bahía Blanca, Argentina

[‡]FICES (UNSL), Avenida 25 de Mayo 384, 5730 Villa Mercedes (San Luis), Argentina

[§]Institut de Tècniques Energètiques, Universitat Politècnica de Catalunya, Avenida Diagonal 647, Ed. ETSEIB, 08028 Barcelona, Spain

ABSTRACT: The implementation of ethane oxidative dehydrogenation (ODH) toward ethylene production in two different reactor configurations is studied here by means of a mathematical model of the reactors. A conventional liquid-cooled multitubular reactor and a multitubular membrane reactor are considered for comparison. Both reactor designs use a Ni−Nb−O catalyst washcoated over raschig-rings inside the tubes; molten salts flow in the shell side of the conventional reactor whereas pure oxygen is assumed for the shell of the membrane reactor. Industrial-scale ethylene production is the aim. Results show that the variation of the bed density (different thickness of the catalytic washcoat over the pellets) shows opposite effects on both reactor designs. For the conventional reactor, the increase in bed density leads to more pronounced hot spots as well as to an undesired oxygen depletion inside the tubes. Conversely, for the membrane reactor, higher bed densities prevent oxygen accumulation along the tube length leading to lower oxygen partial pressures and, consequently, higher selectivities. In this way, higher ethylene production rates are feasible. Although molten salts provides enhanced heat removal, the oxygen injection at only the tube mouth in the conventional reactor leads to lower global selectivities and higher heat generation rates. In the membrane reactor design, the heat generation rate proves to be efficiently controlled by the permeation flow of oxygen through the membrane.

1. INTRODUCTION

Catalytic oxidative dehydrogenation (ODH) of ethane to ethylene is considered nowadays the most attractive alternative route to the classical industrial process of thermal steam cracking.[1,2] Catalytic ethane ODH is exothermic and not equilibrium-limited. When operated over a suitable catalyst, relatively low reaction temperatures are feasible. The reactions proceed via a triangular series/parallel scheme with the undesired complete combustions of both ethane and ethylene. The system of reactions is represented by eqs 1−3:

$$C_2H_6 + \frac{1}{2}O_2 \rightarrow C_2H_4 + H_2O \quad \Delta H_1 = -105\,\frac{kJ}{mol} \qquad (1)$$

$$C_2H_6 + \frac{7}{2}O_2 \rightarrow 2CO_2 + 3H_2O \quad \Delta H_2 = -1428\,\frac{kJ}{mol} \qquad (2)$$

$$C_2H_4 + 3O_2 \rightarrow 2CO_2 + 2H_2O \quad \Delta H_3 = -1323\,\frac{kJ}{mol} \qquad (3)$$

In the ethane ODH process, the yield of ethylene is limited by the total oxidation reactions, namely, the parallel ethane combustion and the in-series ethylene combustion, both forming carbon dioxide. As seen in eqs 2 and 3, total oxidation reactions generate a large amount of heat that can cause a runaway of the reactor and even explosions. At present, intensive research is being carried out to develop both adequate reactor technologies for an effective and safe plant operation[2] and active and selective catalyst formulations.[3−7] As mentioned elsewhere,[8−10] for such exothermic processes, the control of the reaction temperature appears as a key factor to maintain a good selectivity level. The reactor choice and design therefore become outstandingly important. Industry makes extensive use of multitubular reactors to conduct these exothermic processes, with the aim of efficiently removing the generated heat from the catalyst bed. Thousands of tubes of small diameter are employed in order to minimize thermal radial gradients and enhance the ratio between the heat-exchange area and the reaction volume. The bundle of tubes is immersed in a shell through which a proper coolant flows.[8] Lopez et al.[11] reported simulation studies of a multitubular ethane-to-ethylene ODH reactor. Results suggested that the reactor operation would be feasible, provided that high heat transfer area per unit volume and low oxygen concentrations along the tube are maintained. This last consideration proved to be a key factor to achieve adequate selectivity levels leading to high ethylene productions. A two-bed design with the possibility of splitting the oxygen fed between the reactor mouth and an intermediate position was also analyzed, proving a performance enhancement due to the selectivity increase.

An attractive alternative to fixed-bed reactors when a distributed feed is required is the use of a membrane reactor. When applied to the ethane ODH, oxygen can be axially injected in the reaction media leading to lower oxygen partial pressures in the

Special Issue: IMCCRE 2010

Received: March 26, 2010
Accepted: June 22, 2010
Revised: June 17, 2010
Published: August 9, 2010

ACS Publications © 2010 American Chemical Society

dx.doi.org/10.1021/ie100738q | *Ind. Eng. Chem. Res.* 2011, 50, 2690–2697

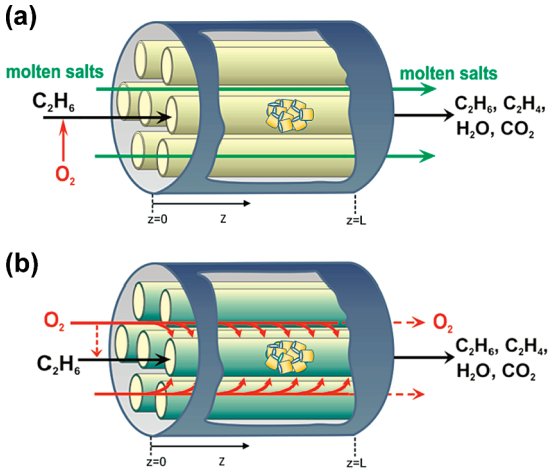

Figure 1. Scheme of the multitubular reactors: (a) conventional reactor (CR) and (b) membrane reactor (MR).

catalyst bed and higher selectivity. The oxygen distribution also allows better heat management, as it leads to a diminution of the local reaction rates and, consequently, of the rate of heat generation.[12−14] The advantages of the application of membrane reactors on ODH at lab scale have been reported for ethane,[12,13,15] propane,[16,17] and butane,[18,19] and literature reviews have also addressed the interest and progress in this field.[20−25] Rodríguez et al.[26,27] reported simulation studies of a multitubular membrane reactor for industrial-scale ethylene production from ethane ODH. Inorganic porous membrane tubes were proposed for the oxygen distribution from the main oxygen stream flowing on the shell side. The membrane tubes were assumed to be packed with catalyst particles. The ODH membrane reactor proved appropriate to reach significant ethylene productions per tube and mild axial temperature profiles. Operating conditions had to be carefully adjusted to avoid undesired oxygen accumulation inside the tubes.

This contribution compares the performance of two different designs of multitubular reactors for the ODH of ethane to ethylene, namely, the conventional reactor (CR) and the membrane reactor (MR). As shown in Figure 1, in the CR the oxygen injection is performed at the tube mouth whereas in the MR the oxygen injection occurs along the tube wall. Both reactor designs are comparatively analyzed and adjusted individually to reach higher ethylene production rates. The performance of a mixed design comprising oxygen feed at both the tube mouth and the tube wall is also addressed.

2. MATHEMATICAL MODEL

A one-dimensional, pseudohomogeneous, steady-state model has been used to represent the ODH of ethane in both multitubular reactors (CR and MR). On the basis of the operation with high total flow rates through the catalyst bed, axial mass and energy dispersions as well as external transport limitations were assumed to be negligible. The use of tubes of small diameter (1 in.) supports the assumption of relatively flat composition and temperature radial profiles. Heat losses from the shell to the environment were neglected. The friction factor f proposed by Ergun was adopted to predict the pressure drop inside the tubes. The catalyst particles were assumed to be washcoated hollow cylinders (Raschig-ring type) of 6 × 6 × 2 mm in order to diminish the pressure drop along the reactor length. A bed void fraction of 0.48 was considered in the simulations, in agreement

Table 1. Parameters of the Membrane[29,30]

$K_0 \times 10^{10}$ [m]	23.1
$B_0 \times 10^{17}$ [m^2]	11.5
δ [m]	0.001 75
k [W/m K] (at T = 300 °C)	16.06

with the literature.[28] The washcoat covering the rings, where the active components are impregnated, was assumed to have a mean thickness of ∼180 μm. Internal mass and energy transport limitations were also neglected due to the low thickness of the washcoat. The use of washcoated particles results in low bed densities when compared to classic values in fixed-bed reactors, favoring the moderation of the heat generation rate per unit volume and, consequently, achieving milder operating conditions.

The allowable maximum temperature (T_{mall}) adopted in the simulations was 425 °C according to catalyst activity tests.[6] An inert ceramic porous membrane was selected for this study as high permeation fluxes are needed, which cannot be provided by dense membranes. The geometric parameters of the membrane and its thermal conductivity[29,30] are reported in Table 1.

As shown in Figure 1, molten salts are selected as cooling medium in the conventional multitubular reactor; properties are taken from Rose.[9] The MR profits from oxygen flowing in the shell, which acts as coolant, besides permeating through the membrane into the catalyst bed. In this context, the MR is assumed to be cooled by both convective heat exchange between reactants and coolant (as in the CR) and by a cold-shot of the oxygen being permeated through the membrane. To avoid multiplicity of steady-states inherent to countercurrent operations, a cocurrent flow configuration between process gas and coolant was assumed. Additionally, the cocurrent scheme lowers down the hot spots, which leads to longer catalyst life and reduces the parametric sensitivity. This ensures safe operational conditions.[31]

The mathematical model describing the behavior of the CR and MR is represented by the following equations:

Reaction Side (catalyst tubes)

Mass Balances

$$\frac{dF_j}{dz} = A_T \rho_B \sum_{i=1}^{3} \nu_{ij} r_i \quad \text{for all } j \text{ values (CR); for } j \neq O_2 \text{ (MR)} \tag{4}$$

with j = C_2H_6, C_2H_4, O_2, H_2O, CO_2

$$\frac{dF_{O_2}}{dz} = A_T \rho_B \sum_{i=1}^{3} \nu_{i,O_2} r_i + J_{O_2} \pi d_T \quad \text{for } j = O_2 \text{ (MR)} \tag{5}$$

Energy Balance

$$\frac{dT}{dz} = \frac{A_T}{\sum_{j=1}^{5} F_j Cp_j} \left[\rho_B \sum_{i=1}^{3} r_i (-\Delta H_{r_i}) - \frac{4}{d_T} (J_{O_2} Cp_{O_2} + U)(T - T_S) \right] \tag{6}$$

where J_{O_2} = 0 (CR) and $J_{O_2} \neq 0$ (MR, eqs 11−13)

dx.doi.org/10.1021/ie100738q |Ind. Eng. Chem. Res. 2011, 50, 2690–2697

Momentum Equation

$$\frac{dP}{dz} = -\frac{f\rho_g {u_s}^2}{d_p} \quad (7)$$

Shell Side:
Mass Balance (for MR):

$$\frac{dF^S_{O_2}}{dz} = -J_{O_2}\pi d_T n_T \quad (8)$$

Energy Balance

$$\frac{dT_S}{dz} = \frac{U\pi d_T n_T (T - T_S)}{F^S_j Cp_j} \quad \text{where}$$

$$j = \text{molten salts (CR); } j = O_2 \text{ (MR)} \quad (9)$$

Initial Conditions

$$\text{at } z = 0: \quad F_j = F_{j0} \quad F^S_j = F^S_{j0} \quad T = T_0$$

$$T_S = T_{S0} \quad P = P_0 \quad (10)$$

The permeation flux of oxygen is quantified by the following expression:[32]

$$J_j = -\frac{1}{RT_m}\left[\frac{D^e_j}{\delta}(p_j - p_{j,S}) + \frac{B_0}{\delta\mu_j} p_{j,S}(P - P_S)\right] \quad j = O_2 \quad (11)$$

$$D^e_j = \left(\frac{1}{D^e_{ij}} + \frac{1}{D^e_{j,k}}\right)^{-1} \quad (12)$$

$$D^e_{j,k} = K_0\sqrt{\frac{8RT}{\pi M_j}} \quad (13)$$

The power-law kinetic model proposed by Heracleous and Lemonidou[7] for the reactions 1−3 over a $Ni_{0.85}Nb_{0.15}O$ catalyst was used for the simulations. The overall-heat transfer coefficient (U) was evaluated using the guidelines suggested in Froment and Bischoff.[33] The heat-transfer coefficient for the process gas side was calculated by means of the equation of Leva[34] and that corresponding to the shell side by the expressions reported by Kern.[35] The global selectivity (S_G) was calculated as the ratio between the amount of ethylene produced and the amount of ethane consumed, from the reactor inlet to the desired axial coordinate:

$$S_G = \frac{F_{C_2H_4,z} - F_{C_2H_4,0}}{F_{C_2H_6,0} - F_{C_2H_6,z}} \quad (14)$$

Table 2 reports the design parameters of both MR and CR along with the main operating conditions.

3. RESULTS AND DISCUSSION

3.1. Comparison between Conventional and Membrane Reactors. To compare the performances of the CR and the MR, the number of moles of ethane being converted per unit time is kept constant (300.55 kmol C_2H_6/h). The geometrical parameters and operating conditions are given in Table 2. Figure 2 shows the temperature profiles for CR and MR. In the CR design, the molten salts preheat the feed in the first 50 cm of the tubes (filled with inert particles) and downstream act as a coolant medium.[11] This way of feed preheating is usual in industry. Although a slight hot spot appears for $z \cong 3.2$ m, the reaction temperature is appropriately controlled due to the high heat removal rates.

In the case of MR, the feed temperature is considerably higher ($T_0 = 380$ °C) and the O_2 stream is considered entering the shell at 25 °C. The permeation flux through the membrane is varied by applying different trans-membrane pressure drops ($\Delta P_{T\text{-}M}$). This was done by adjusting the pressure on the shell side. To

Table 2. Geometrical Parameters and Operating Conditions

	reactor	
parameters	CR	MR
L	4 m (inert solid in the first 0.50 m)	4 m
d_T	0.0266 m	0.0266 m
d_S	3.93 m	3.93 m
n_T	10 000	10 000
ρ_B	50 kg_{cat}/m^3bed	50 kg_{cat}/m^3bed
d_P	0.0045 m	0.0045 m
catalyst type	hollow cylinders	hollow cylinders
coolant	molten salts	pure O_2
$F_{0,T}$	3000 kmol/h	3000 kmol/h
$F_{0,S}$	300 kg/s	24.1 kg/s
T_0	100 °C	380 °C
T_{S0}	312−363 °C	25 °C
P_0	5 atm	5 atm
P_{0S}	n.a.	5.3−6.147 atm
y_{0,O_2}	0.1	0
y_{0,C_2H_6}	0.9	1
baffles number	3	3
bed number	1	1

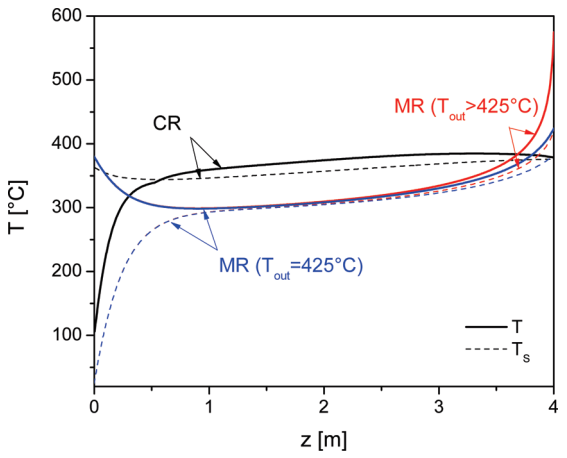

Figure 2. Tube-side (solid lines) and shell-side (dashed lines) temperatures vs axial position for CR (at T_0 = 100 °C, T_{S0} = 363 °C, inlet O_2 = 10%, ρ_B = 50 kg_{cat}/m^3 bed) and MR (at T_0 = 380 °C, T_{S0} = 25 °C, inlet O_2 = 0%, ρ_B = 50 kg_{cat}/m^3 bed, P_{0S} = 6.147 atm for T_{out} > 425 °C and P_{0S} = 6.065 atm for T_{out} = 425 °C. Remaining conditions as in Table 2).

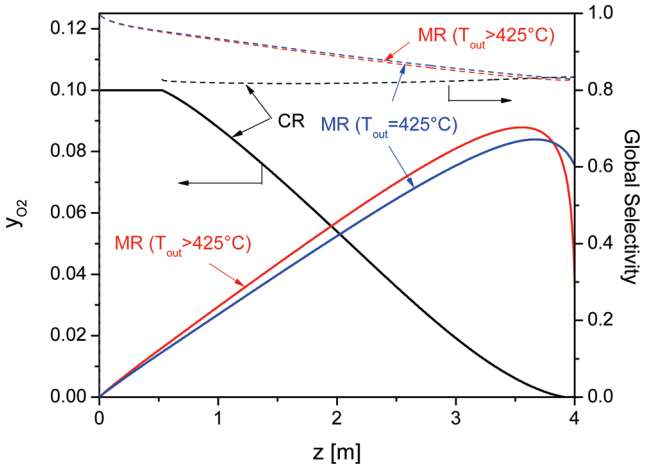

Figure 3. Oxygen molar fraction profiles along the reactor length, for the conditions of Figure 2. Right ordinate axis: global selectivity.

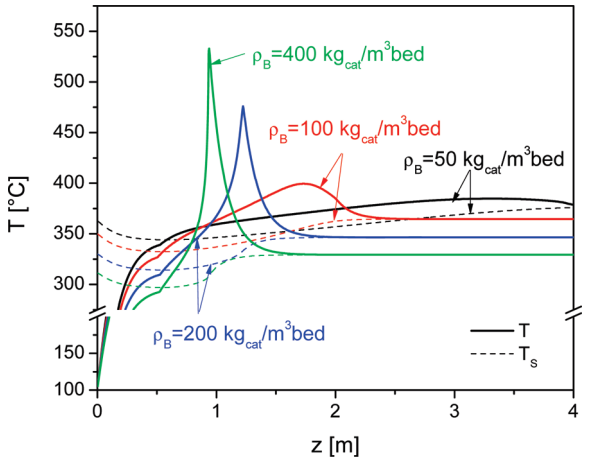

Figure 4. Tube-side (solid lines) and shell-side (dashed lines) temperatures vs axial position for CR (at T_0 = 100 °C, inlet O_2 = 10%, ρ_B = 50, 100, 200, and 400 kg_{cat}/m^3 bed, T_{S0} = 312, 330, 350, and 363 °C, respectively).

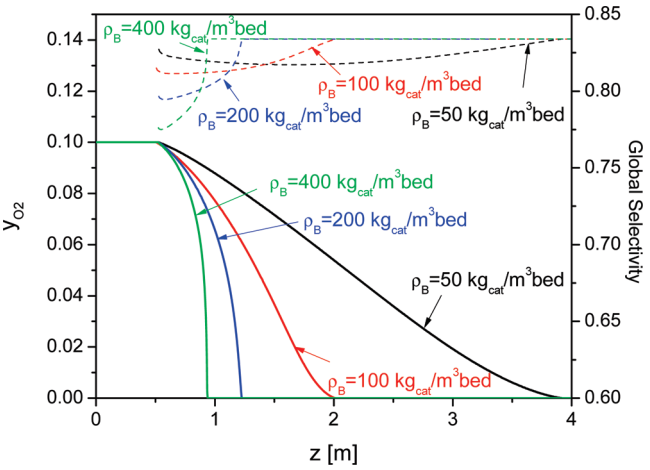

Figure 5. Oxygen molar fraction along the reactor length for CR with different bed densities (ρ_B = 50, 100, 200, and 400 kg_{cat}/m^3 bed). Right ordinate axis: global selectivity.

reach the same quantity of converted ethane that in CR, it is necessary to use trans-membrane pressure drops ($\Delta P_{T\text{-}M}$) higher than 1 atm (P_{0S} = 6.147 atm). As shown, the outlet temperature overcomes the maximum allowable temperature according to the catalyst test (Figure 2, upper solid curve for MR). If the pressure on the shell side is adjusted to satisfy T_{mall} = 425 °C, (P_{0S} = 6.065 atm, lower solid curve), the MR proves to be unable to convert the quantity of moles of ethane fixed on a comparison basis. This high outlet temperature observed in the MR is a consequence of both the predominance of the exothermic combustion reactions and the poor heat capacity of the gas flowing on the shell side.

This behavior can be explained by means of Figure 3, in which the axial profiles of oxygen molar fraction for both reactors are presented at the same conditions of Figure 2.

The O_2 consumption for CR starts at z = 0.50 m because of the presence of inerts in the preheating zone. An O_2 depletion near the reactor outlet is observed. For the two operating conditions corresponding to MR in Figure 3, the higher the final temperatures are, the lower O_2 concentrations are found at the reactor outlet region. In both cases the presence of remnant O_2 at the reactor end is observed. This accumulation phenomenon represents a clearly undesired situation that is caused by the low reaction rates at hand. The right ordinate axis of Figure 3 shows global selectivities for the CR and the MR. The high O_2 concentration at the reactor mouth in the CR leads to an initially poorer selectivity; lower O_2 partial pressures toward the reactor end are not sufficient to recover the selectivity values. For the MR cases, global selectivities diminish monotonically with z, due to the high O_2 accumulation inside the tubes. The operating conditions selected here do not allow taking advantage of the MR's ability to work at low partial pressures of O_2 in order to improve global selectivity and ethylene yield. In the next subsections, the operating conditions are adjusted, with the aim of improving the performance of both reactor designs.

3.2. Influence of Bed Density (ρ_B). To analyze the influence of the bed density for both reactor designs, the thickness of the active layer in the washcoated catalyst particle is varied, whereas the dimensions of the pellet remain the same. Figures 4 and 5 show the axial temperature profiles for CR at four different values of bed density: ρ_B = 50, 100, 200, and 400 kg_{cat}/m^3 bed. The coolant inlet temperature (T_{S0}) is varied in order to keep constant the amount of ethane being converted (300.55 kmol C_2H_6/h). As shown in Figure 4, the increase in the bed density for the CR leads to pronounced hot-spots due to the fast evolution of the reaction rates, even though the molten salts enters the reactor gradually at lower temperatures. As ρ_B is increased, the O_2 consumption along the reactor becomes faster and the O_2 depletion shifts the reactor entrance, as a consequence of the higher reaction rates per unit volume (Figure 5). In real application, this condition is not convenient, not only because the catalyst in this zone renders unused, but also because secondary reactions will ignite using oxygen from the catalyst lattice, leading to a gradual reduction of the catalyst and to coke formation.[36] The outlet selectivity is not affected significantly by the bed density (Figure 5, right axis); therefore, the ethylene production remains constant (Table 3). Clearly, increasing the bed density is not suitable for the CR.

Figure 6 shows axial temperature profiles for the MR for the same values of bed density (ρ_B = 50, 100, 200, and 400 kg_{cat}/m^3 bed), whereas Figure 7 reports the corresponding oxygen composition axial profiles and selectivities. The pressure on the shell side was adjusted here for each bed density in order to attain the

Table 3. Operative Parameters of CR for the Conditions of Figure 4

reactor design	CR			
ρ_B [kg_{cat}/m^3 bed]	50	100	200	400
ethane converted [kmol C_2H_6/h]	300.55	300.49	300.57	300.59
total O_2feed [kmol/h]	300	300	300	300
T_{max} [°C]	384.78	399.49	476.00	532.94
L (T_{max}) [m]	3.31	1.73	1.22	0.94
C_2H_4 production [ton/year]	56 145	56 128	56 145	56 154

Table 4. Operative Parameters of MR for the Conditions of Figure 6

reactor design	MR			
ρ_B[kg_{cat}/m^3 bed]	50	100	200	400
ethane converted [kmol C_2H_6/h]	300.52	300.46	300.55	300.71
total O_2 feed (by permeation) [kmol/h]	429.57	229.68	197.5	182.05
T_{max} [°C]	574.82	470.57	434.11	416.8
L (T_{max}) [m]	4	4	4	4
C_2H_4 production [ton/year]	55 789	61 173	63 656	64 410

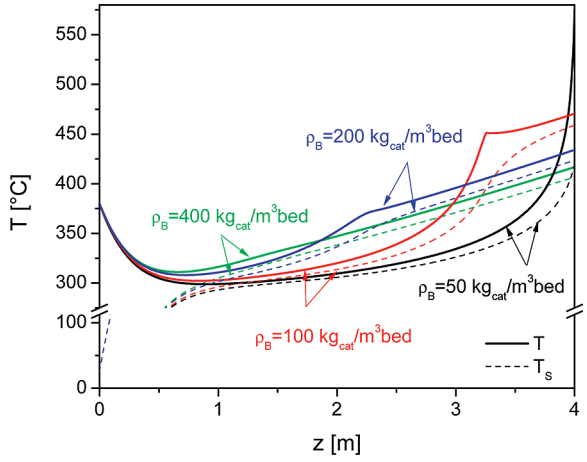

Figure 6. Tube-side (solid lines) and shell-side (dashed lines) temperatures vs axial position for MR (at T_0 = 380 °C, T_{S0} = 25 °C, inlet O_2 = 0%, ρ_B = 50, 100, 200, and 400 kg_{cat}/m^3 bed).

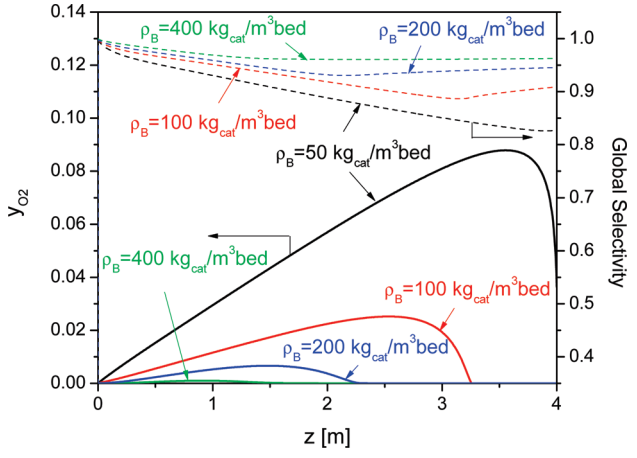

Figure 7. Oxygen molar fraction along the reactor length for the conditions of Figure 6. Right ordinate axis: global selectivity.

same ethane converted inside the tubes as in CR (300.55 kmol/h). After a minimum is shown, the temperature reaches its maximum value at the reactor outlet, for the four curves, clearly surpassing the allowable maximum temperature for the lower densities. As ρ_B increases, O_2 accumulation inside the tubes tends to disappear (see Figure 7), i.e., the conversion of O_2 is practically complete for $\rho_B \geq 100$ kg_{cat}/m^3 bed. Nevertheless, it is important to note that the O_2 permeated through the membrane permanently oxidizes the catalyst sites avoiding coke formation. The lower O_2 partial pressures on the reaction side favor the

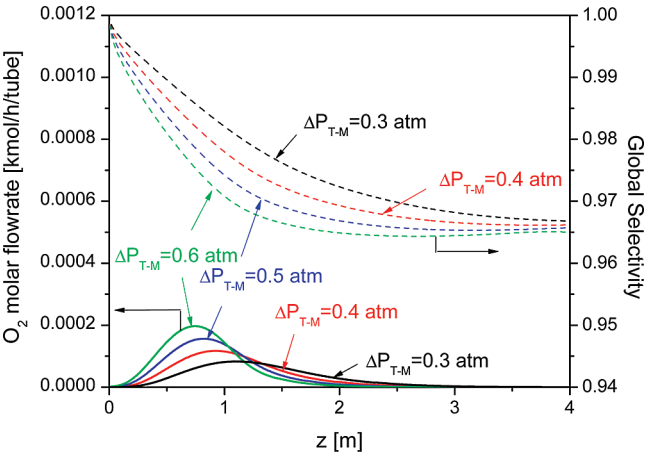

Figure 8. Oxygen molar flow rate along the reactor length for different trans-membrane pressure drops ($\Delta P_{T\text{-}M}$ = 0.3, 0.4, 0.5, and 0.6 atm; ρ_B = 400 kg_{cat}/m^3 bed). Right ordinate axis: global selectivity.

ODH's reaction (higher global selectivity; see Figure 7, right coordinate axis). The increases in the reaction rate and the global selectivity lead to an enhance in ethylene production, as reported in Table 4. It is interesting to compare the results for different bed densities: higher ρ_B values lead simultaneously to the same ethane converted, less O_2 converted (see stoichiometry), and substantially lower maximum temperatures (see Table 4 and Figures 6 and 7). The decrease in the maximum temperature ("inverse response" with respect to the bed density) is a consequence of the improvement in selectivity, i.e., the less exothermic ODH reaction is being favored. Conversely to the CR, the selection of higher bed densities improves the MR performance. By comparison of Tables 3 and 4, the ethylene production rates of the MR (ton/year) are higher than those of CR, provided that $\rho_B \geq 100$ kg_{cat}/m^3 bed.

3.3. Influence of the Oxygen Permeation Flux. As it is referred to in a previous subsection, the permeation flux through the membrane is varied by applying different trans-membrane pressure drops ($\Delta P_{T\text{-}M}$). This was done by adjusting the pressure on the shell side to satisfy the desired $\Delta P_{T\text{-}M}$ value. Figure 8 shows the influence of the parameter $\Delta P_{T\text{-}M}$ on the axial profiles of oxygen molar flow rate and global selectivity. The increase in trans-membrane pressure drops leads to higher oxygen permeation rates, and an accumulation of O_2 in the first tube section is observed. This causes a slight drop of the global selectivity (see Figure 8, right axis). Despite this, since the reaction rates are high enough and the selectivity is not too deteriorated, a substantial increase in the ethylene production is obtained by the $\Delta P_{T\text{-}M}$ values, as shown in Figure 9. It is important to note that the production rate is determined by the permeated oxygen. In fact,

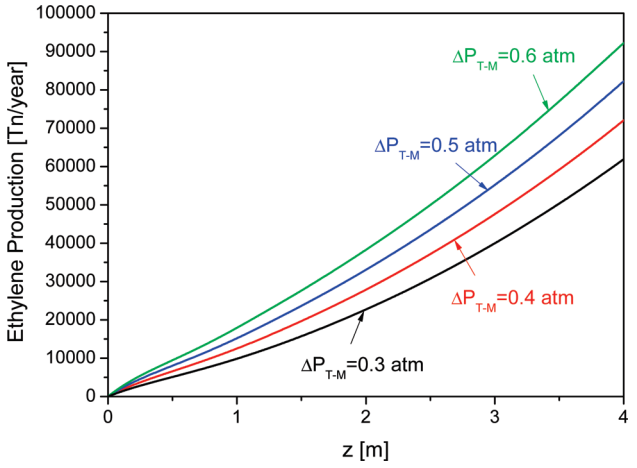

Figure 9. Ethylene production profiles for the same conditions of Figure 8.

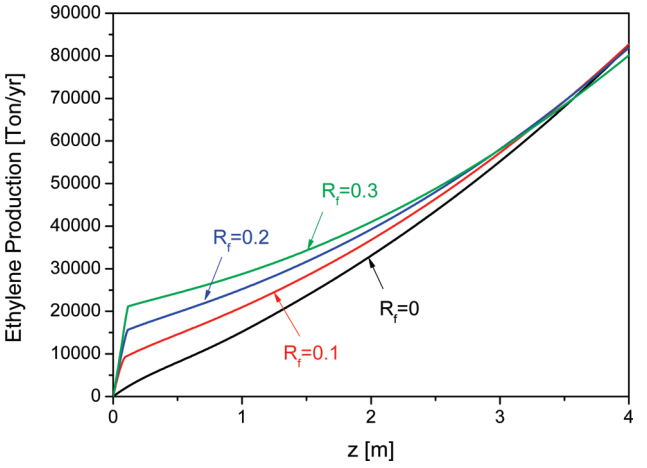

Figure 11. Ethylene production profiles for the same conditions of Figure 10.

Table 5. Outlet Temperatures for the Conditions of Figure 8

$\Delta P_{T\text{-}M}$ [atm]	0.3	0.4	0.5	0.6
T [°C]	402.27	418.5	432.95	448.3

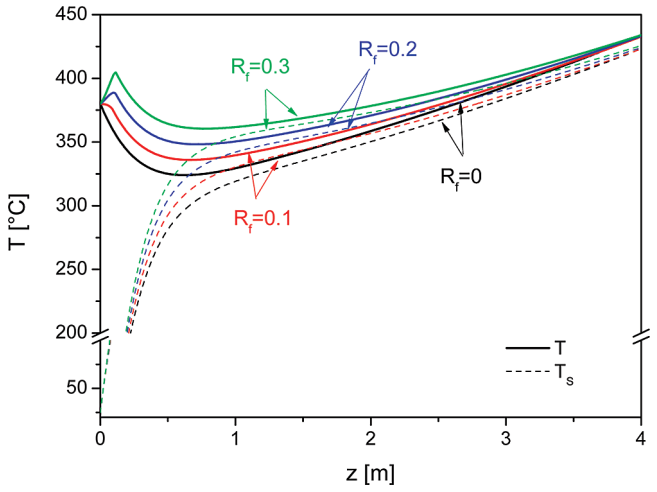

Figure 10. Tube-side (solid lines) and shell-side (dashed lines) temperatures profiles for different O_2 feed ratios (R_f = 0, 0.1, 0.2, and 0.3).

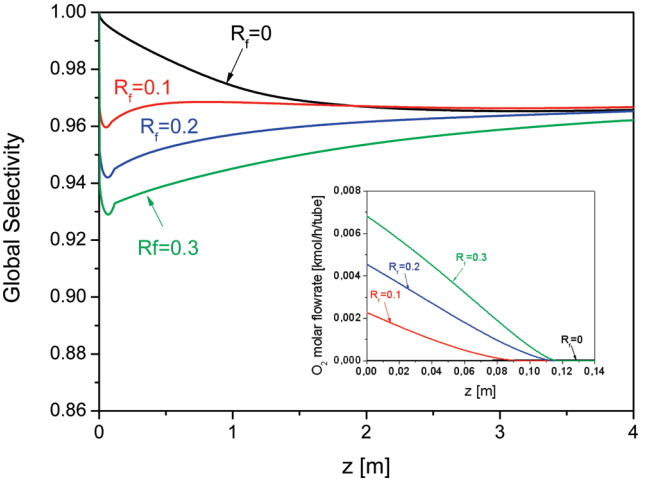

Figure 12. Global selectivity profiles for the same conditions of Figure 10. Figure detail: oxygen molar flow rate along the reactor length.

the outlet production rate increases around 49% when the transmembrane pressure drop is increased from 0.3 to 0.6 atm. However, Table 5 shows that the outlet temperature for the cases of $\Delta P_{T\text{-}M}$ = 0.5 and 0.6 slightly exceeds the allowable maximum temperature (425 °C).

3.4. Influence of the Oxygen Feed Distribution. A combination of the CR and the MR with respect to the oxygen feed policy can be analyzed. In fact, we present here studies regarding a MR with oxygen feed both in the tube mouth as well as the tube wall. The parameter R_f represents the ratio between the oxygen being fed at the reactor inlet ($F_{O_2}{}^0$) and the total oxygen feed ($F_{O_2}{}^T$); i.e., $R_f = F^0{}_{O_2}/F_{O_2}{}^T$. A new comparison basis is adopted, namely, the total flow rate of oxygen fed to the reactor is kept constant ($F_{O_2}{}^T$ = 227 kmol/h). The remaining operating conditions are given in Table 2. Figure 10 shows the temperature profiles along the reactor length for different oxygen feed distributions. Again, the pressure on the shell side is adjusted to modify the permeation rate through the membrane to maintain, in this case, the fixed total feed of oxygen. For R_f = 0.2 and 0.3, a small hot-spot is observed near the reactor inlet and the temperature minima observed in Figure 10 (all for R_f = 0) tend to disappear. The outlet (maximum) temperature is similar for all R_fs. When O_2 is fed at the tube mouth (R_f = 0.1−0.3), a fast ignition of the reactions is verified, as shown in the axial ethylene production rates reported in Figure 11. After the initial O_2 depletion, the rate of O_2 consumption by chemical reaction is nearly balanced with the rate of permeation through the membrane. As a result, no accumulation of O_2 is found in the catalyst bed. The increase of oxygen fed at the reactor mouth (higher R_f) leads to an initial decrease of the global selectivity, as shown in Figure 12. This initial loss cannot be recovered in the zones where the O_2 partial pressures are low enough. As a consequence the outlet ethylene production diminishes slightly (see Figure 11). It suggests the existence of an optimal R_f ratio that leads to low O_2 partial pressures without an irrecoverable deterioration of the global selectivity in the initial section.

dx.doi.org/10.1021/ie100738q |*Ind. Eng. Chem. Res.* 2011, 50, 2690–2697

4. CONCLUSIONS

The results lead to the following conclusions: (1) The increase in bed densities has opposite effects on both designs. Higher bed density values for the CR lead to hot-spots due to the fast evolution of the reaction rates. In order to maintain mild temperature profiles inside the tubes as ρ_B is increased, it is necessary to diminish the inlet coolant temperature (T_{S0}). Nevertheless the final reactor zone with O_2 depletion still remains; this is a clearly not a convenient situation.

Conversely to the CR, higher bed densities improve the MR performance and lead to an increase of the reaction rates. O_2 accumulation inside the tubes tends to disappear due to an increase in the O_2 consumption rate. Low O_2 partial pressures on the reaction side favor the ODH's reaction (high global selectivity). The predominance of the least exothermic reaction (ODH of ethane) allows better temperature control. The augment of the reactions rates and global selectivity causes an increase in ethylene production.

(2) A convenient selection of the R_f ratio leads to lower oxygen partial pressures inside the catalyst tubes, which result in an improved ethylene yield.

(3) The increase in O_2 consumption rate for the unit of volume allows increasing the O_2 permeation flux across the membrane leading to higher ethylene production rates. However, the maximum temperature can be exceeded.

(4) Because of the high heat capacity of the molten salts and good shell side heat transfer coefficients, the CR is very efficient to remove the reaction heat from the reaction tubes, provided that low reaction rates per unit volume occur. However, feeding all the O_2 at the reactor inlet does not help to maintain high selectivity to ethylene and low heat generation rates. Conversely, the MR is capable to reach high selectivity and ethylene production, because of the lower oxygen partial pressures along the tubes. The reaction rate, i.e., the heat generation rate, can be controlled by means of the permeation flow through the membrane. This is a powerful tool to improve the temperature control, whether a better coolant medium than the proper oxygen stream can be employed in the shell side. Another interesting possibility to improve temperature control is the use of a fluid-bed cooled packed-bed membrane reactor with a feed of oxygen from the fluid bed to the packed bed.[37,38] These last options remain as challenges for an optimum reactor design in ethane ODH.

AUTHOR INFORMATION

Corresponding Author

*E-mail: mlrodriguez@plapiqui.edu.ar.

NOMENCLATURE

A_T = cross sectional area of tubes, m^2
B_0 = geometric parameter of the membrane, m^2
Cp_j = specific heat of component j, kJ/ (kmol K)
d_P = equivalent diameter of the catalyst pellet (momentum equation), m
d_T = internal tube diameter, m
d_T = internal tube diameter, m
d_S = shell diameter, m
d_S = shell diameter, m
D^e_{ij} = effective molecular diffusion coefficient of component j, m^2/s
$D^e_{j,k}$ = effective Knudsen diffusion coefficient of component j, m^2/s
D^e_j = Bosanquet diffusion coefficient of component j, m^2/s
E_i = activation energy of reaction i, kJ/mol
f = friction factor, dimensionless
F_j = molar flow of component j (reaction side), kmol/h
F^S_j = molar flow of component j (shell side), kmol/h
F_T = = total molar flow rate, kmol/h
F_S = total molar flow rate, shell side, kmol/h
J_j = permeation flow of component j, kmol/(h m^2)
k_m = membrane thermal conductivity, W/m K
K_0 = geometric parameter of the membrane, m
M_j = molecular weight of component j, kg/kmol
n_T = number of tubes
L = tube length, m
p_j = partial pressure of component j (tube side), Pa
P = total pressure (reaction side), Pa
P_S = total pressure (shell side), Pa
P_m = average pressure, Pa
r_i = reaction rate, reaction i, $kmol_{CH}/(kg_{cat}\ s)$ where $HC{=}C_2H_6$ (reactions 1 and 2) and $HC{=}C_2H_4$ (reaction 3)
R = universal gas constant, kg $m^2/(kmol\ s^2\ K)$
S_G = global selectivity, dimensionless
T = temperature (reaction side), K
T_m = average temperature, K
T_{mall} = allowable maximum temperature, K
T_{max} = maximum temperature, K
T_{out} = outlet temperature, K
T_S = temperature (shell side), K
U = overall heat transfer coefficient, kJ/(h m^2 K)
u_s = superficial velocity, $m_f^3/(m_r^2\ s)$
y_j = molar fraction, mol_j/mol_{total}
z = axial coordinate, m

Greek letters

α = heat transfer coefficient, kJ/(h m^2 K)
δ = membrane thickness, m
ΔH_{ri} = heat of reaction i, kJ/mol
$\Delta P_{T\text{-}M}$ = pressure drop across the membrane, atm
ρ_g = gas density, kg/m_f^3
ρ_B = bed density, kg_{cat}/m^3 bed
μ_j = viscosity of component j, Pa s

Subscripts and Superscript

i = reaction i
j = component j
0 = at the axial coordinate $z = 0$
L = at the axial coordinate $z = L$
S = shell side
T = tube side
C_2H_6 = ethane
C_2H_4 = ethylene
CO_2 = carbon dioxide
H_2O = water
O_2 = oxygen

REFERENCES

(1) Centi, G.; Cavani, F.; Trifiró, F. *Selective Oxidation by Heterogeneous Catalysis*; Kluwer Academic Publishers/Plenum Press: New York, 2001.

(2) Cavani, F.; Ballarini, N.; Cericola, A. Oxidative dehydrogenation of ethane and propane: How far from commercial implementation? *Catal. Today* **2007**, *127*, 113.

(3) Bañares, M. A. Supported metal oxide and other catalysts for ethane conversion: a review. *Catal. Today* **1999**, *51*, 319.
(4) Cavani, F.; Trifiró, F. Selective oxidation of light alkanes: interaction between the catalyst and the gas phase on different classes of catalytic materials. *Catal. Today* **1999**, *51*, 561.
(5) Grabowski, R. Kinetics of Oxidative Dehydrogenation of C_2-C_3 Alkanes on Oxide Catalysts. *Catal. Rev.* **2006**, *48*, 199.
(6) Heracleous, E.; Lemonidou, A. A. Ni-Nb-O mixed oxides as highly active and selective catalysts for ethene production via ethane oxidative dehydrogenation. Part I: Characterization and catalytic performance. *J. Catal.* **2006**, *237*, 162.
(7) Heracleous, E.; Lemonidou, A. A. Ni-Nb-O mixed oxides as highly active and selective catalysts for ethene production via ethane oxidative dehydrogenation. Part II: Mechanistic aspects and kinetic modeling. *J. Catal.* **2006**, *237*, 175.
(8) Arpentinier, P.; Cavani, F.; Trifiro, F. *The Technology of Catalytic Oxidations*; Technip: Paris, France, 2001.
(9) Rose, L. M. *Chemical Reactor Design in Practice*; Elsevier Scientific Pub. Co.: New York, 1981.
(10) Eigenberger, G. *Fixed-bed reactors, Ullmann's Encyclopedia of Industrial Chemistry*, Vol. B4; VCH Publishers: Weinheim, Germany, 1992.
(11) López, E.; Heracleous, E.; Lemonidou, A. A.; Borio, D. O. Study of a multitubular fixed-bed reactor for ethylene production via ethane oxidative dehydrogenation. *Chem. Eng. J.* **2008**, *145*, 308.
(12) Coronas, J.; Menéndez, M.; Santamaría, J. Use of a Ceramic Membrane Reactor for the Oxidative Dehydrogenation of Ethane to Ethylene and Higher Hydrocarbons. *Ind. Eng. Chem. Res.* **1995**, *34*, 4229.
(13) Tonkovich, A. L. Y.; Zilka, J. L.; Jimenez, D. M.; Roberts, G. L.; Cox, J. L. Experimental investigations of inorganic Membrane reactors: a distributed feed approach for partial oxidation reactions. *Chem. Eng. Sci.* **1996**, *51*, 789.
(14) Téllez, C.; Menéndez, M.; Santamaría, J. Simulation of an inert membrane reactor for the oxidative dehydrogenation of butane. *Chem. Eng. Sci.* **1999**, *54*, 2917.
(15) Klose, F.; Wolff, T.; Thomas, S.; Seidel-Morgenstern, A. Operation modes of packed-bed membrane reactors in the catalytic oxidation of hydrocarbons. *Appl. Catal., A* **2004**, *257*, 193.
(16) Pantazidis, A.; Dalmon, J. A.; Mirodatos, C. Oxidative dehydrogenation of propane on catalytic membrane reactors. *Catal. Today* **1995**, *25*, 403.
(17) Ramos, R.; Menéndez, M.; Santamaría, J. Oxidative dehydrogenation of propane in an inert membrane reactor. *Catal. Today* **2000**, *56*, 239.
(18) Téllez, C.; Menéndez, M.; Santamaría, J. Oxidative dehydrogenation of butane using membrane reactors. *AIChE J.* **1997**, *43*, 777.
(19) Ge, S. H.; Liu, C. H.; Wang, L. J. Oxidative dehydrogenation of butane using inert membrane reactor with a non-uniform permeation pattern. *Chem. Eng. J.* **2001**, *84*, 497.
(20) Sanchez-Marcano, J. G.; Tsotsis, T. T. *Catalytic Membranes and Membrane Reactors*; Wiley-VCH: Weinheim, Germany, 2002.
(21) Coronas, J.; Santamaría, J. Catalytic reactors based on porous ceramic membranes. *Catal. Today* **1999**, *51*, 377.
(22) Julbe, A.; Farrusseng, D.; Guizard, C. Porous ceramic membranes for catalytic reactors—overview and new ideas. *J. Membr. Sci.* **2001**, *181*, 3.
(23) Dixon, A. G. Recent Research in Catalytic Inorganic Membrane Reactors. *Int. J. Chem. React. Eng.* **2003**, *1*, 1(Review R6).
(24) Saracco, G.; Neomagnus, H. W. J. P.; Versteeg, G. F.; van Swaaij, W. P. M. High-temperature membrane reactors: potential and problems. *Chem. Eng. Sci.* **1999**, *54*, 1997.
(25) Sirkar, K. K.; Shanbhag, P. V.; Kovvali, A. S. Membrane in a Reactor: A Functional Perspective. *Ind. Eng. Chem. Res.* **1999**, *38*, 3715.
(26) Rodríguez, M. L.; Ardissone, D. E.; Lemonidou, A. A.; Heracleous, E.; López, E.; Pedernera, M. N.; Borio, D. O. Simulation of a Membrane Reactor for the Catalytic Oxidehydrogenation of Ethane. *Ind. Eng. Chem. Res.* **2009**, *48*, 1090.
(27) Rodríguez, M. L.; Ardissone, D. E.; Heracleous, E.; Lemonidou, A. A.; López, E.; Pedernera, M. N.; Borio, D. O. Oxidative dehydrogenation of ethane to ethylene in a membrane reactor: A theoretical study. *Catal. Today* DOI: 10.1016/j.cattod.2010.01.053.
(28) Marsella, A.; Fatutto, P.; Carmello, D. *Catalyst and oxychlorination process using it*. U.S. Patent 6,465,701, October 15, 2002.
(29) Pedernera, M.; Mallada, R.; Menéndez, M.; Santamaría, J. Simulation of an Inert Membrane Reactor for the Syntesis of Maleic Anhydride. *AIChE J.* **2000**, *46*, 2489.
(30) Munro, R. G. Evaluated material properties for a sintered α-alumina. *J. Am. Ceram. Soc.* **1997**, *80*, 1919.
(31) Borio, D. O.; Gatica, J. E.; Porras, J. A. Wall-cooled fixed-bed reactors: Parametric sensitivity as a design criterion. *AIChE J.* **1989**, *35*, 287.
(32) Mallada, R. Ph.D. Thesis, University of Zaragoza, Spain, 1999.
(33) Froment, G. F.; Bischoff, K. B. *Chemical Reactor Analysis and Design*; Wiley: Toronto, Canada, 1990.
(34) Leva, M. Fluid flow through packed tubes. *Chem. Eng.* **1949**, *56*, 115.
(35) Kern, D. Q. *Procesos de Transferencia de Calor*; Compañía Editorial Continental: México, 1997.
(36) A. A. Lemonidou, personal communication, 2009.
(37) Ramos, R.; Pina, M. P.; Menéndez, M.; Santamaría, J.; Patience, G. S. Oxidative dehydrogenation of propane to propene, 2: Simulation of a commercial inert membrane reactor immersed in a fluidized bed. *Can. J. Chem. Eng.* **2001**, *79*, 902.
(38) Alonso, M.; Lorences, M. J.; Pina, M. P.; Patience, G. S. Butane partial oxidation in an externally fluidized bed-membrane reactor. *Catal. Today* **2001**, *67*, 151.